Geophysical Research Letters

Supporting Information for

Impact of ocean resolution on coupled air-sea fluxes and large-scale climate

Malcolm J. Roberts[1], Helene T. Hewitt[1], Pat Hyder[1], David Ferreira[2], Simon A. Josey[3], Matthew Mizielinski[1], Ann Shelly[1,4]

[1] Met Office, Fitzroy Road, Exeter. EX1 3PB, UK

[2] Department of Meteorology, University of Reading, Reading, RG6 6BB, UK

[3] National Oceanography Centre, Southampton, SO14 3ZH, UK

[4] Now at Cumulus, City Financial Investment Company Limited, London EC4R 1EB, UK

Contents of this file

Introduction

The text under S1 describes the methodology for the spatial filtering including the code. Figure S1 shows the scatter plot of SST and wind stress for different ocean basins, with Fig. S2 showing the spatial structure of the filtered fields, to give a comparison with previously published work. Text S2 and Fig. S3 describes the correlation and regression of the filtered SST and wind stress using only the winter hemisphere months, when the relationship is stronger. Text S3 uses a simple bulk formula for latent heat flux to show that SST is the main component in the difference in latent heat flux between the different resolution models. Figure S4 shows the SST-latent heat flux scatter plot relationship, and Fig. S5 the differences in latent heat flux due to components of the bulk formula.

Text S1.

Following *Maloney and Chelton* [2006] and *Bryan et al.* [2010], in order to isolate the mesoscale (high pass filtered) signal of interest we remove the smoothed field generated by filtering. These previous studies used a Loess filter, while here we use a box car filter with dimensions 18° longitude by 6° latitude. The box car filter is simple and efficient to implement in python, and the code used is this study, together with an example field, is available at

https://github.com/robertsmalcolm/primavera-code-repository

In order to demonstrate that this produces similar results to the above studies using Loess filtering, Fig. S1 shows the spatially filtered fields of SST and wind stress in both the Gulf Stream and Agulhas regions, to be compared for example to Fig. 1 of *Chelton and Xie* [2010] and Fig. 2 of *Bryan et al.* [2010]. It is clear that the structures and magnitudes are very similar, despite the use of different datasets and different methodology.

To quantify relationships between the frontal scale SST features and those in wind stress, we construct binned scatterplots. The procedure is to group the SST data from the monthly means of the daily high-pass filtered fields into bins of 0.1°C, and then calculate bin averages and standard deviations of the associated points from the filtered wind stress field. A least squares linear fit is calculated from each of these monthly mean fields, and the mean and standard deviation of this fit is used in the final seasonal plot, referred to as the coupling coefficient. Monthly means are used in order to isolate the time-invariant structures (mesoscale fronts and standing eddies) from the transient moving structures (e.g. eddies, filaments).

The scatter plots from the Agulhas and Kuroshio regions for DJF and JJA are shown in Fig. S2. The Kuroshio plot shares characteristics with the Gulf Stream plot (Fig. 1) with the models having a significantly weaker coupling coefficient compared to the observations by about 50%, though the higher resolution model has a slightly stronger value. For the Agulhas region, the coefficient is stronger than found over the northern hemisphere boundary currents, and the models' coupling coefficients are somewhat closer to those observed (only 20% too weak). This may be due to the different characters of the frontal structures, with the Agulhas region featuring a retroflection and standing eddies rather than a western boundary current and lateral boundary.

Text S2.

Since the SST-wind stress relationship is weaker in the summer hemisphere, this could impact on the correlations shown in Fig. 2. Hence we show in Fig. S3 the correlation (left column) and regression (right column) using only months from the winter season in each hemisphere (December-January-February for northern and July-July-August for southern hemisphere respectively). As expected, there are wide spread positive correlations that extend further from the boundary currents, in particular near the Kuroshio and the Gulf Stream. However there is a similar difference between the model resolutions as seen in the annual plots. In order to gain insight into the spatial distribution of the coupling coefficient in global terms, Fig. S3 shows the SST-wind stress regression for the models and observations using the winter hemisphere monthly mean filtered fields. The strongest coupling coefficients are found in the Southern Ocean over wide areas with values above 0.25, with stronger values found in the N512-O12 simulation compared to the lower resolution model. The higher resolution model agrees well with the observationally-based datasets over the Southern Ocean, but lacks the high regression values over the western boundary current regions, which as before is likely due to a weaker wind stress response.

Text S3.

The large-scale circulation, the air-sea coupling strength and surface heat fluxes have the potential to interact and feed back on each other [*Ma et al*. 2016; *Wu et al*. 2016], and here we attempt to understand cause and effect. Figure S4 shows the total net heat flux from DEEP-C, together with differences to show spread amongst observations (OAFlux) and biases in the models. The notable increase in heat flux south of the Gulf Stream is most likely due to the increased SST (indicated by the contours), resulting from earlier and improved separation of the boundary current from the coastline in the eddy-resolving model [*Chassignet and Marshall*, 2008 and others], and hence likely to be via latent heat fluxes.

In order to support the argument that the additional heat loss to the south of the Gulf Stream is due to latent heat, and due to the increase in SST, we use a simple bulk formula calculation; based on the approach of OAFlux [*Yu et al*., 2008]. Using the COARE 3.0 algorithm [*Fairall et al*., 2003], the latent heat flux equation is

$$Q_{LH} = \rho L_e c_e U (q_s - q_a) \quad (1)$$

$$q_s = 0.98 q_{sat} (T_s)$$

where Q_{LH} is the latent heat flux, U is the relative wind speed, q_s and q_a are the surface and near surface relative humidities, respectively. q_{sat} is the saturation humidity for pure water at T_s, the sea surface skin temperature, and $\rho L_e c_e$ are the density of air, latent heat of evaporation and turbulent exchange coefficient for latent heat respectively.

Fig. S5 shows the difference in the model latent heat flux at different resolutions (positive upwards), together with the latent heat flux difference derived from this bulk formula, using long-term DJF mean values of each variable from the models. This shows that the bulk formula-derived flux in Fig. S5(b) describes the large majority of the difference in the modelled latent heat in Fig. S5(a). If we then examine the difference in the bulk formula latent heat due to the SST and the near surface humidity (by substituting each of these values into the bulk formula in turn from the N216-O025 model, leaving the other values from the N512-O12), it is clear that the main difference comes from the surface temperature difference between the models. Note that this also highlights that the path of the boundary current is further south in the N512-O12 model.

Given the above we would expect the SST and latent heat flux to be closely related in the models. Fig. S6 shows the SST-latent heat scatter plot calculated as previously for SST-windstress. The model resolution has minimal impact on this coupling coefficient, suggesting around 20 Wm-2 additional latent heat flux for every 1°C SST change, consistent with the above calculation and SST contours shown in Fig. S4. This relationship is much tighter than seen in the SST-wind stress, as measured by the standard deviation of the fit in each bin. It is also more asymmetric at positive and negative temperature anomalies than the SST-wind stress relationship.

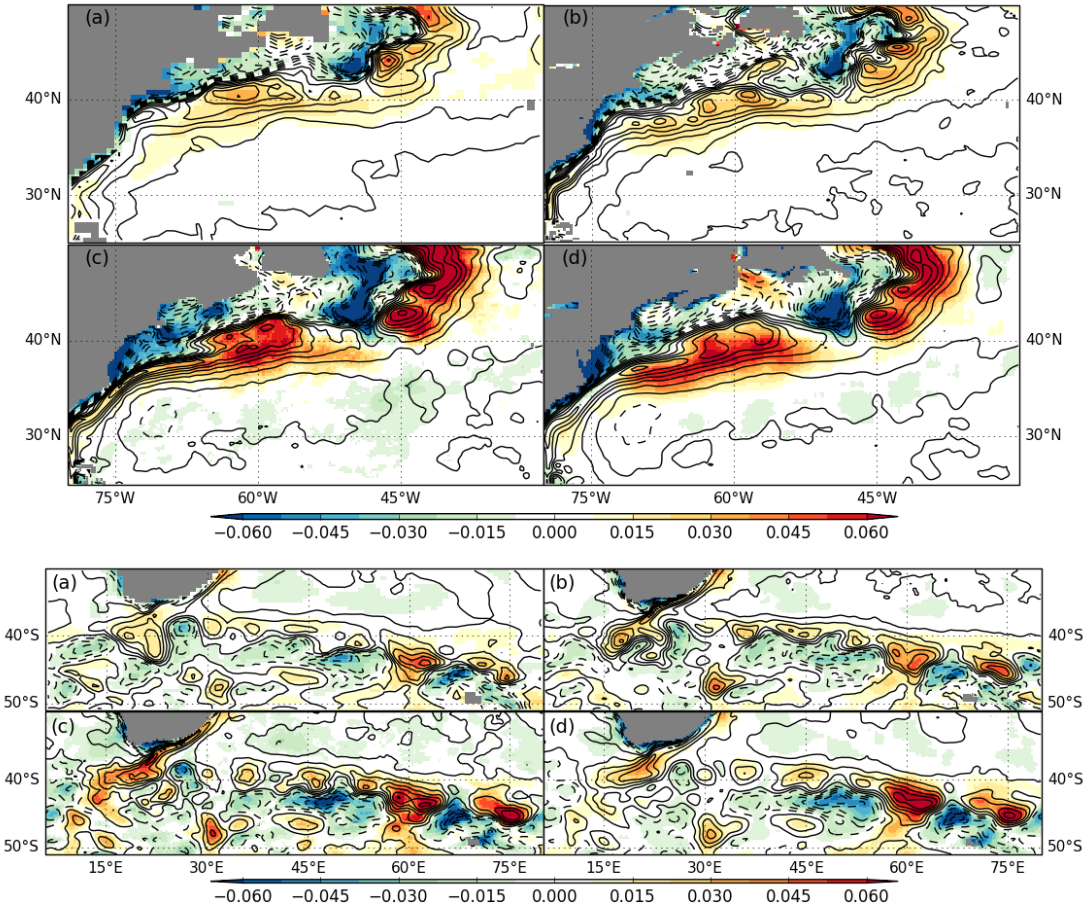

Figure S1. Monthly mean of daily high pass filtered wind stress (colours) and SST (contours) for winter season from (top) Gulf Stream and (bottom) Agulhas regions from models and observations/reanalyses. (**a**) N216-O025; (**b**) N512-O12; (**c**) QuikScat-CCI SST; (**d**) CCMP-OISST.

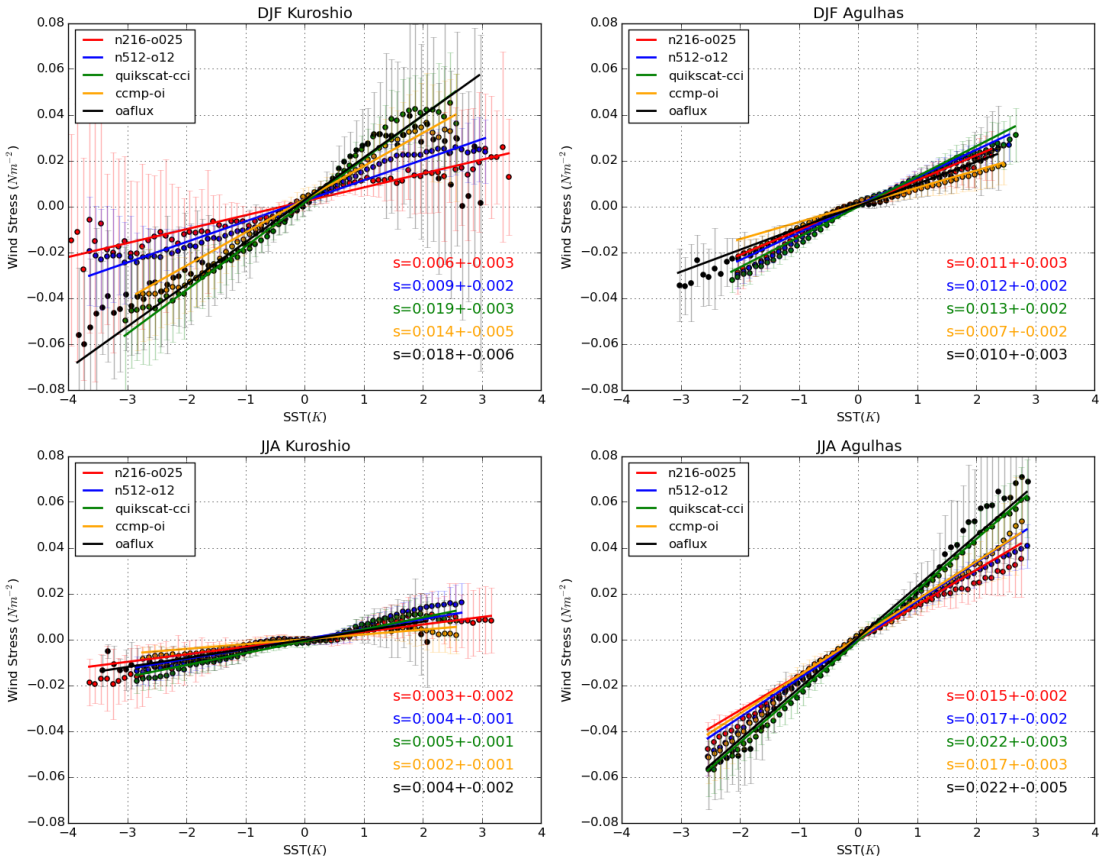

Figure S2. Binned scatterplots of high pass filtered SST and wind stress with the linear regression coefficient indicated. This regression is derived from the mean of each monthly mean distribution over the region and season indicated. Red is the N216-O025 model and blue is N512-O12. There are three pairs of observationally-based data: ESA-CCI SST and QuikSCAT windstreses; OISST and CCMP wind stresses; OAFlux surface temperature and wind stress. Error bars on the scatter plot are derived from the combined standard deviation of each monthly mean field, while for the regression the error is derived from the standard deviation of each monthly linear fit.

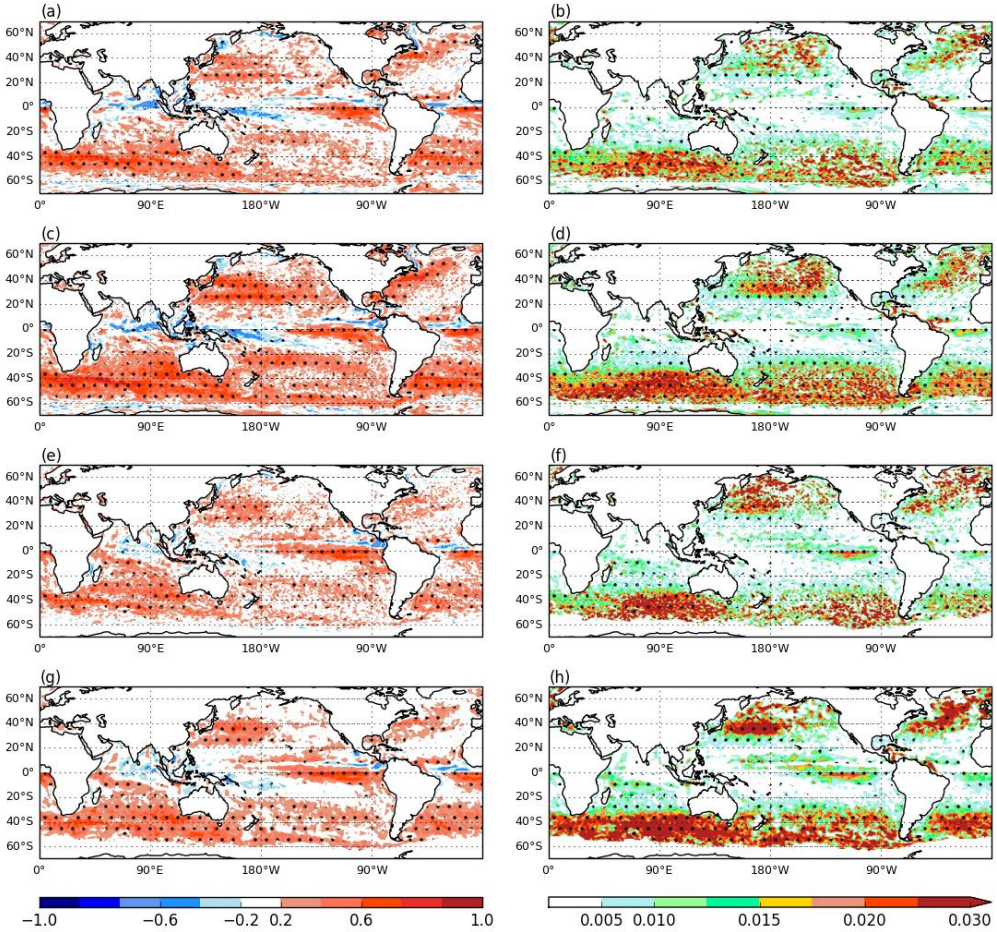

Figure S3. (left column) Correlation of the timeseries of monthly mean high pass spatially filtered SST and wind stress derived from the daily data; (right column) Regression coefficient using the same data as (left column). Only months from the winter hemisphere are used. (**a**), (**b**) N216-O025; (**c**), (**d**) N512-O12; (**e**), (**f**) OISST and CCMP wind stress; (**g**), (**h**) OAFlux surface temperature and wind stress. Hatching indicates significance at the 95% level.

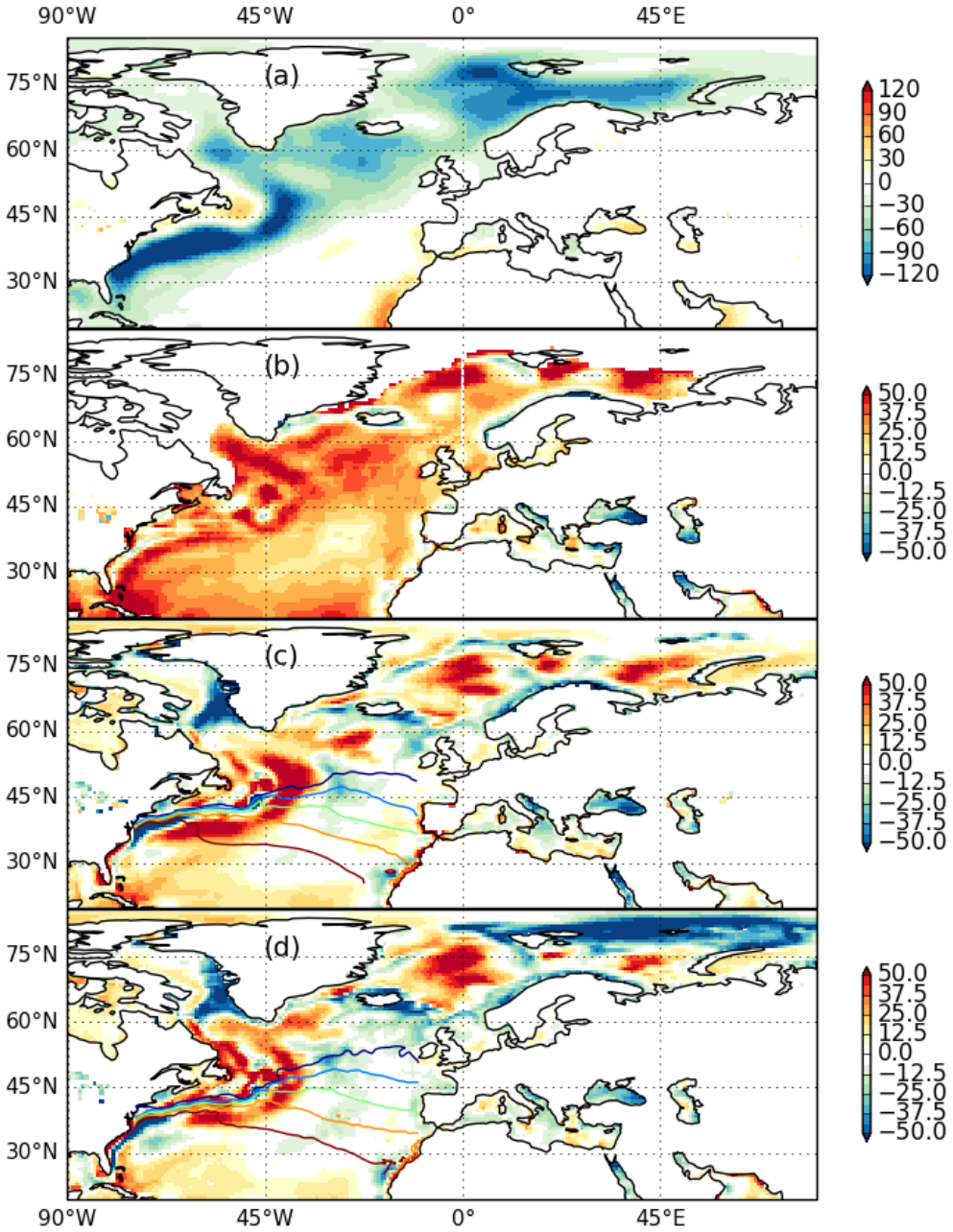

Figure S4. (a) Total net surface heat flux from DEEP-C; (b) difference between DEEP-C and OAFlux total net heat flux; (c) bias in total net surface flux in N216-O025 relative to DEEP-C; (d) as (c) for N512-O12. Units Wm^{-2}. Coloured lines are the annual mean SST contours at 13,15,17,19,21 ˚C from the respective models.

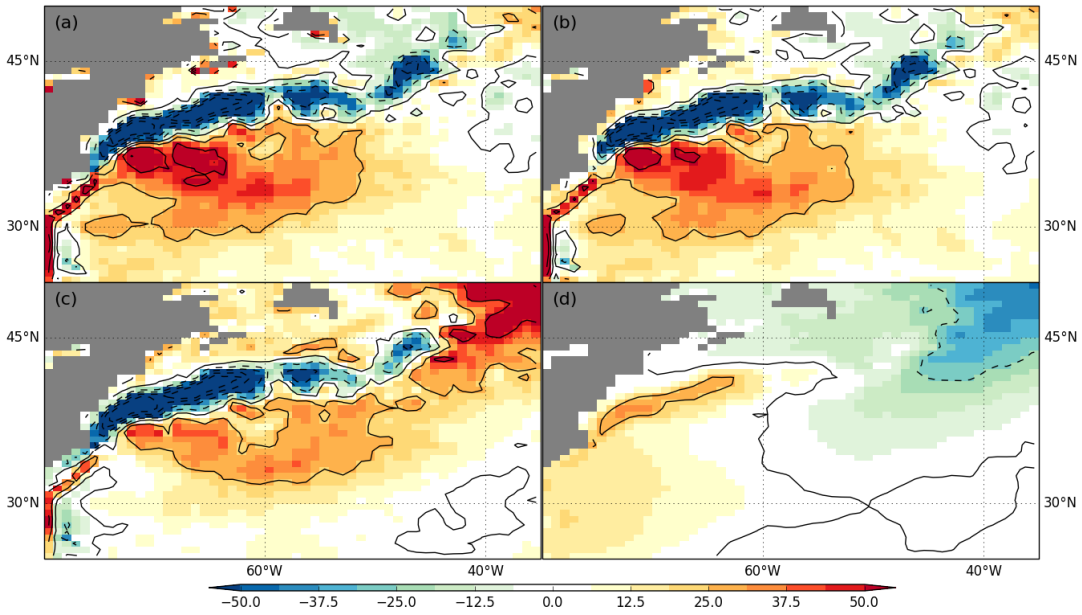

Figure S5. The latent heat flux difference of the 10 year DJF mean, N512-O12 – N216-O025. (**a**) Difference in model latent heat flux (positive upwards) between N512O12 and N216O025. (**b**) Difference in latent heat flux between models as calculated using the bulk formula in (1). (**c**) Component of the bulk formula difference due to SST; (**d**) Component of the bulk formula difference due to specific humidity.

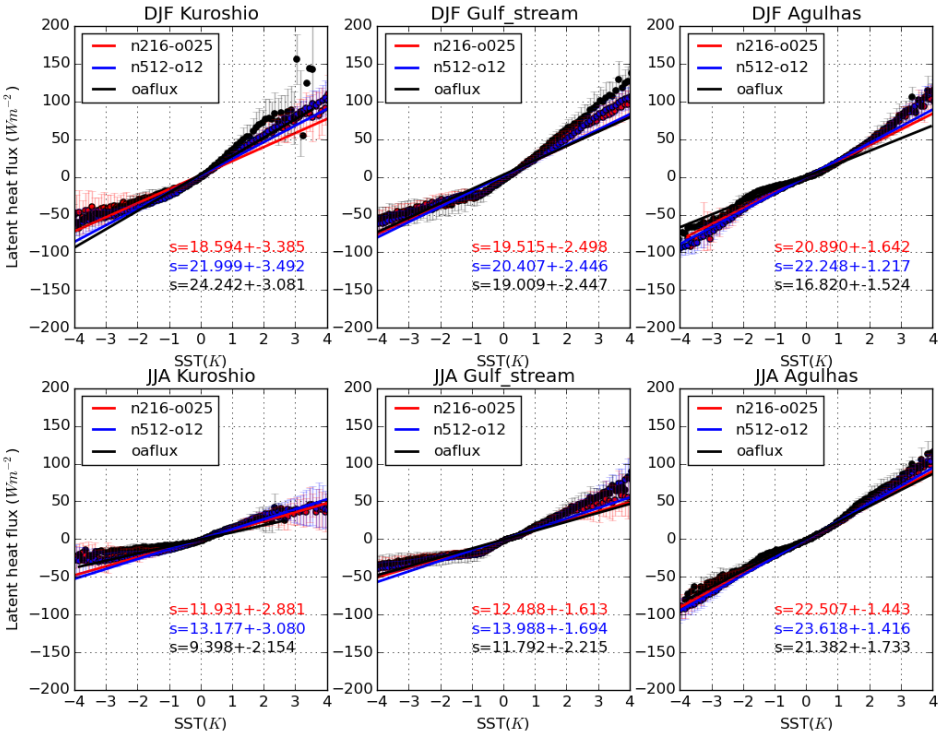

Figure S6. Binned scatterplots of high pass filtered SST and latent heat flux with the linear regression coefficient indicated. This regression is derived from the mean of each monthly mean distribution over the region and season indicated. Red is the N216-O025 model, blue is N512-O12, and black is OAFlux surface temperature and wind stress. Error bars on the scatter plot are derived from the combined standard deviation of each monthly mean field, while for the regression the error is derived from the standard deviation of each monthly linear fit.

Dataset\ Season	N216-O025	N512-O12	QuikSCAT-CCI	CCMP-OISST	OAFlux
Gulf Stream DJF JJA	0.009±0.002 0.004±0.001	0.009±0.001 0.005±0.001	0.016±0.004 0.007±0.001	0.013±0.004 0.004±0.001	0.014±0.003 0.005±0.001
Kuroshio DJF JJA	0.006±0.003 0.003±0.002	0.009±0.002 0.004±0.001	0.019±0.003 0.005±0.001	0.014±0.005 0.002±0.001	0.018±0.006 0.004±0.002
Agulhas DJF JJA	0.011±0.003 0.015±0.002	0.012±0.002 0.017±0.002	0.013±0.002 0.022±0.003	0.007±0.002 0.017±0.005	0.010±0.003 0.022±0.005

Table S1. SST-wind stress linear regression using the 18° x 6° box car filter in each region, for seasons DJF and JJA. Fit is based on the mean fit of each scatter plot from the component monthly mean relationship, and error estimate from the standard deviation of these individual monthly fits.